The Astrophysical Journal, 795:60 (10pp), 2014 November 1 doi:10.1088/0004-637X/795/1/60

MOST SUB-ARCSECOND COMPANIONS OF *KEPLER* EXOPLANET CANDIDATE HOST STARS ARE GRAVITATIONALLY BOUND

Elliott P. Horch[1,5,6,7], Steve B. Howell[2,6,7], Mark E. Everett[3,6,7], and David R. Ciardi[4,6,7]
[1] Department of Physics, Southern Connecticut State University, 501 Crescent Street, New Haven, CT 06515, USA; horche2@southernct.edu
[2] NASA Ames Research Center, Moffett Field, CA 94035, USA; steve.b.howell@nasa.gov
[3] National Optical Astronomy Observatory, 950 North Cherry Avenue, Tucson, AZ 85719, USA; everett@noao.edu
[4] NASA Exoplanet Science Institute, California Institute of Technology, 770 South Wilson Avenue, Mail Code 100-22, Pasadena, CA 91125, USA; ciardi@ipac.caltech.edu
Received 2014 March 16; accepted 2014 September 2; published 2014 October 14

ABSTRACT

Using the known detection limits for high-resolution imaging observations and the statistical properties of true binary and line-of-sight companions, we estimate the binary fraction of *Kepler* exoplanet host stars. Our speckle imaging programs at the WIYN 3.5 m and Gemini North 8.1 m telescopes have observed over 600 *Kepler* objects of interest and detected 49 stellar companions within ∼1 arcsec. Assuming binary stars follow a log-normal period distribution for an effective temperature range of 3000–10,000 K, then the model predicts that the vast majority of detected sub-arcsecond companions are long period ($P > 50$ yr), gravitationally bound companions. In comparing the model predictions to the number of real detections in both observational programs, we conclude that the overall binary fraction of host stars is similar to the 40%–50% rate observed for field stars.

Key words: binaries: visual – planetary systems – stars: solar-type – techniques: high angular resolution – techniques: interferometric – techniques: photometric

1. INTRODUCTION

The *Kepler* mission has confirmed several hundred exoplanets, and has flagged thousands of stars as "Objects of Interest" (KOIs), that is, stars exhibiting a transit-like event in their light curve. Most of these stars are thought to harbor one or more exoplanets, but there will be some false positives, caused by either periodic stellar phenomena or the presence of an unresolved object within the same *Kepler* pixel as the object of interest, such as a background eclipsing binary. Determining whether the signals obtained by *Kepler* are caused by an exoplanet requires a detailed analysis of the light curve (e.g., Lissauer et al. 2014, and references therein) as well as ground-based follow-up observations, including spectroscopy (e.g., Everett et al. 2013) and high-resolution imaging (e.g., Adams et al. 2012; Howell et al. 2011), to rule out as much parameter space for false positives as possible.

A number of recent papers have discussed the links between occurrence and planet properties in relation to single stars and in terms of stellar multiplicity. *Kepler* data has provided an important impetus for work in this area. For example, planet occurrence studies looking at the general trend of planet radii discovered by *Kepler* are contained in Howard et al. (2012) and Fressin et al. (2013). The latter reference summarizes a number of previous and concurrent studies as a function of planet radius from Earth-size to giant planets, in particular concluding that about one in six main sequence stars in the F through K spectral range has an Earth-sized planet with a period of less than 85 days. Regarding the issue of stellar multiplicity, several studies indicate that the presence of a stellar companion will affect planetary formation (e.g., Xie et al. 2010; Kraus et al. 2012; Parker & Quanz 2013). Wang et al. (2014a, 2014b) discuss planet formation and occurrence and the second reference provides a very good summary of approximately a dozen previous works on the subject of host star multiplicity using a range of observational techniques including spectroscopy, adaptive optics, and lucky imaging.

The work presented here involves high-resolution imaging using the technique of speckle imaging. Due to the use of electron-multiplying CCD cameras in recent years, the technique can deliver diffraction-limited images of stellar targets over a broad range of stellar brightness with relatively high dynamic range. For example, stellar companions up to 3–4 mag fainter than a target star can be seen in the visible range within 0.1 arcsec of the target star in many cases at the WIYN 3.5 m Telescope[8] for targets as faint as 13–14th magnitude (see Horch et al. 2010). The upper limit for the separation of components typically observed with speckle imaging is on the order of 1 arcsec; this is usually set by the field of view of the speckle camera and/or the lack of isoplanicity at larger separations. For wider separations, it is possible to search for companions using traditional imaging methods. Speckle imaging can therefore be useful in learning whether KOIs have stellar companions from the diffraction limit of a large ground-based telescope (20–40 mas) up to ∼1 arcsec. Given that KOIs lie mainly between ∼200 pc and ∼1 kpc of the Sun, this translates into range of projected separations of a few to ∼1000 AU.

The known log-normal period distribution for solar-type field binaries has its peak at 180 yr (Duquennoy & Mayor 1991; Raghavan et al. 2010). In rough terms, this period implies a semi-major axis on the order of 40 AU, with about two-thirds of binaries having semi-major axes between a few and 200 AU.

[5] Adjunct Astronomer, Lowell Observatory.
[6] Visiting Astronomer, Gemini Observatory, National Optical Astronomy Observatory, which is operated by the Association of Universities for Research in Astronomy, Inc., under a cooperative agreement with the NSF on behalf of the Gemini partnership: the National Science Foundation (United States), the Science and Technology Facilities Council (United Kingdom), the National Research Council (Canada), CONICYT (Chile), the Australian Research Council (Australia), Ministério da Ciência, Tecnologia e Inovañao (Brazil), and Ministerio de Ciencia, Tecnología e Innovación Productiva (Argentina).
[7] Visiting Astronomer, Kitt Peak National Observatory, National Optical Astronomy Observatory, which is operated by the Association of Universities for Research in Astronomy, Inc. (AURA) under cooperative agreement with the National Science Foundation.
[8] The WIYN Observatory is a joint facility of the University of Wisconsin-Madison, Indiana University, Yale University, and the National Optical Astronomy Observatories.

Comparing with the numbers above, this illustrates that speckle imaging of stars is therefore an excellent way to learn more about binary statistics in this region of the Galaxy in general, including the dependence of binary parameters on spectral type, metallicity, and age. The advent of the KOI data sets (Borucki et al. 2011; Batalha et al. 2013; Burke et al. 2014) represents a group of stars where most members probably host an exoplanet or system of exoplanets. If a subsample of KOIs that have confirmed exoplanets and bound stellar companions can be identified, this would be an important tool in understanding the relationship between binarity and planetary systems. In this paper, we simulate the observable properties of a sample of KOIs (in terms of magnitude and separation), and compare to the speckle imaging data obtained so far on KOIs. This sets the stage for further work to more rigorously and systematically identify binaries with exoplanets from the *Kepler* data set.

2. OBSERVATIONAL SAMPLE

Since 2008, our group has been taking speckle observations of KOIs with the Differential Speckle Survey Instrument (Horch et al. 2009). The camera records speckle images in two filters simultaneously, so that each observation results in two diffraction-limited image reconstructions of the target. In the first channel of the instrument, we have always used a 692 nm filter with a width of 40 nm. However, in the second channel, we have used both an 880 nm with filter width of 50 nm and a 562 nm filter of width 40 nm. While the 562 nm filter gives superior resolution images (owing to its shorter wavelength), we find that the 880 nm filter often gives images with a larger dynamic range, and is therefore sensitive to the detection of fainter companions. In a small number of cases, high-quality data only exist at 692 nm for the target because the data in the other channel were degraded by a scattered light problem in the instrument that has since been resolved. As such, the only filter where all targets observed have data is 692 nm, and this represents our most comprehensive data set.

The basic observing strategy has been to obtain data on as many KOI targets as possible on each observing run, although we have tended to observe targets whose planetary candidate (or at least one of the planetary candidates) is "Earth-sized," i.e., having a derived radius less than about 3 Earth radii. We have rarely repeated observations on these stars, even those with discovered companions, up to this point. For the vast majority of cases, this means we have only one observation in 692 nm and one other observation in one of the other two filters mentioned above. We have found sub-arcsecond companions to 49 *Kepler* stars out of a grand total of over 600 observed at present, combining results from both the WIYN 3.5 m Telescope at Kitt Peak and the Gemini North 8.1 m Telescope on Mauna Kea. As we will discuss further in Sections 4 and 5, a number of these are expected to be false positives; current information on the CFOP Web site[9] indicates that of these stars, 74 have been judged to be false positives (12%), 11 of which are found to be binary in our speckle observations. This latter number represents 22% of those stars detected as binary so far.

Since the speckle data that we have is in two filters, it would in principle be possible to put the components of any binary or multiple stars detected onto the H-R diagram to test whether a common isochrone is consistent with the positions of the stars. However, the speckle analysis of WIYN data has been shown to give magnitude differences between components with uncertainties in the 0.1–0.2 mag range for a wide range of component brightnesses (see, e.g., Figure 7 in Horch et al. 2010). Therefore, the color information that we have at present is uncertain to 0.14–0.28 mag, depending on signal-to-noise ratio and other factors. As such, in the vast majority of cases, we do not have sufficient leverage on the component colors to attempt an analysis of this type at present. Likewise, with a sufficient number of observations over a period of years, it would be possible in principle to detect orbital motion, or common proper motion, based on data obtained from the speckle camera. However, we do not yet have the data necessary for this analysis because of the observing strategy mentioned above; only a handful of stars have multiple observations. We show in Table 1 details of the observations obtained at WIYN and Gemini North. More information on the speckle observing process can be found in Howell et al. 2011 and Horch et al. 2011 (WIYN) and Horch et al. 2012 (Gemini). A more detailed analysis of these systems including final relative astrometry and photometry, as well as placement of components on the H-R diagram, will be forthcoming when sufficient follow-up data exist.

Table 1
Basic Properties of the Observed Data Set

Parameter	WIYN	Gemini
Total observations	682	42
Stars observed	588	35
Average *Kepler* magnitude of sample	12.85	13.04
Companions detected	41	8
Stars with multiple observations	60	2
Stars with 880 nm filter data	453	35
Stars with 562 nm filter data	135	0

We have excluded Gemini observations of three KOIs in this study, namely those of KOI 98, KOI 284, and KOI 2626. The first two of these objects were known to be double from WIYN observations, and the Gemini observation was made to confirm the earlier result and compare data quality directly with the WIYN observations. These objects only appear in the figures presented here of WIYN data and in the WIYN statistics displayed in Table 1. We have observed the third object, KOI 2626, on three occasions at Gemini, but this object is removed from consideration here as those observations were to confirm Adaptive Optics results that had already been obtained at the Keck Observatory. This object was never observed at WIYN, and does not appear anywhere in the data presented here.

In Figures 1 and 2, we show further properties of the observed sample for both telescopes. In Figure 1, we show the placement of objects in the *Kepler* field; this illustrates that the samples are consistent with a random distribution in terms of sky position. In Figure 2, we show the *Kepler* magnitude of the stars as a function of estimated distance; drawing upon Huber et al. 2014, a distance modulus is obtained from the spectral type implied from the effective temperature and known surface gravity of the star and inferring an absolute magnitude from that. This does not account for the binarity or multiplicity of some of the stars in the sample, which would affect the estimated distance and stellar properties to some degree depending on the magnitude difference of the components; the distances obtained are intended only to show that, in rough terms, the sample of observed stars is similar to the simulation results. Finally, in Figure 3, we show the surface gravity as a function of effective temperature; this shows that while the sample spans a range in effective temperature from

[9] See https://cfop.ipac.caltech.edu/home/.

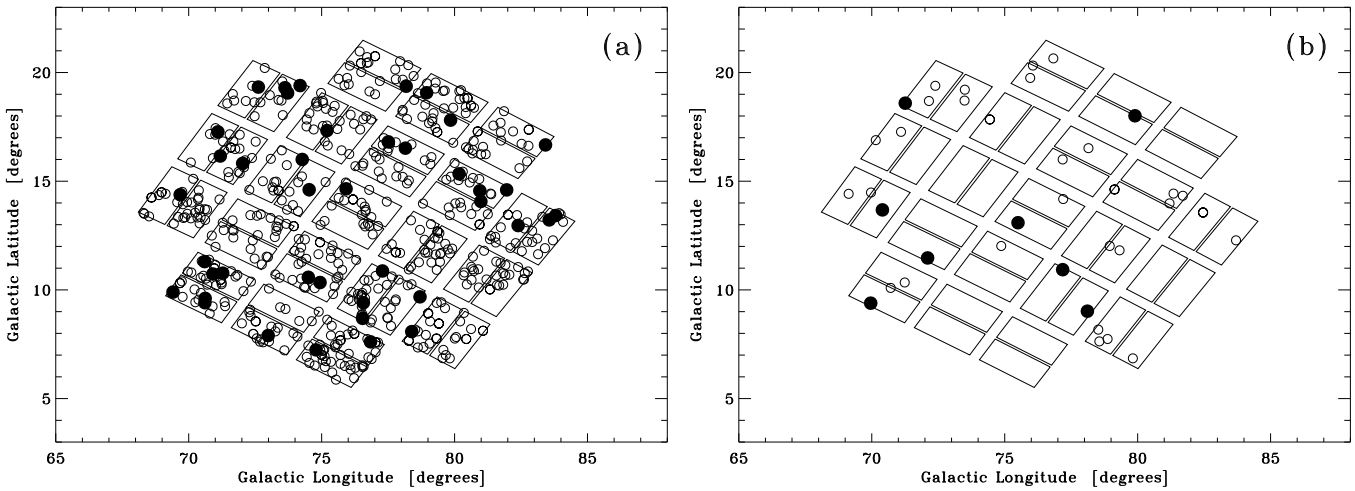

Figure 1. Location in galactic coordinates for the stars observed at (a) WIYN, and (b) Gemini. Open circles represent stars not found to have companions from the speckle observations, and filled circles represent stars where a companion has been detected. The outline of the *Kepler* CCDs is shown by rectangular shapes drawn with solid lines.

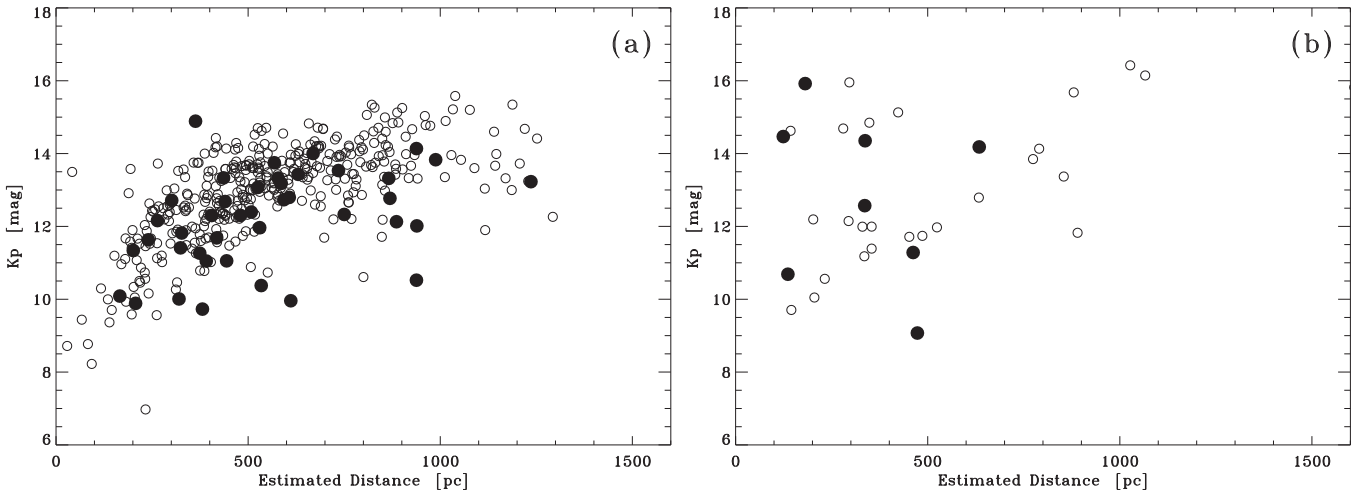

Figure 2. *Kepler* magnitude as a function of estimated distance for the sample of stars observed at (a) WIYN and (b) Gemini. Open circles represent stars with no detection of a companion, and filled circles represent stars with detected companions.

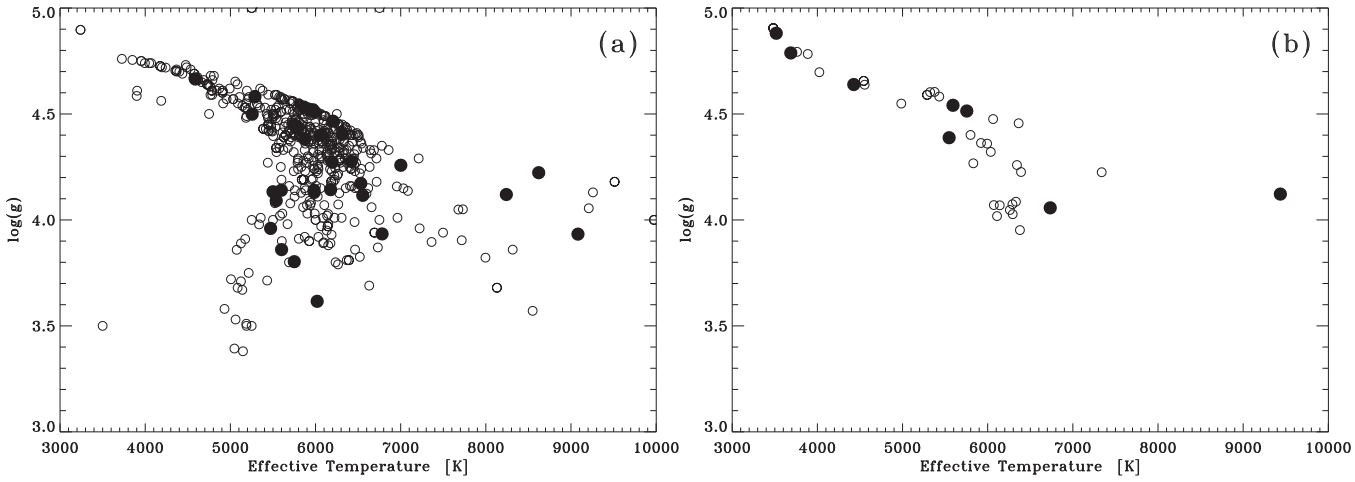

Figure 3. Surface gravity [log(g)] as a function of effective temperature for the sample of stars observed at (a) WIYN and (b) Gemini. Open circles represent stars with no detection of a companion, and filled circles represent stars with detected companions.

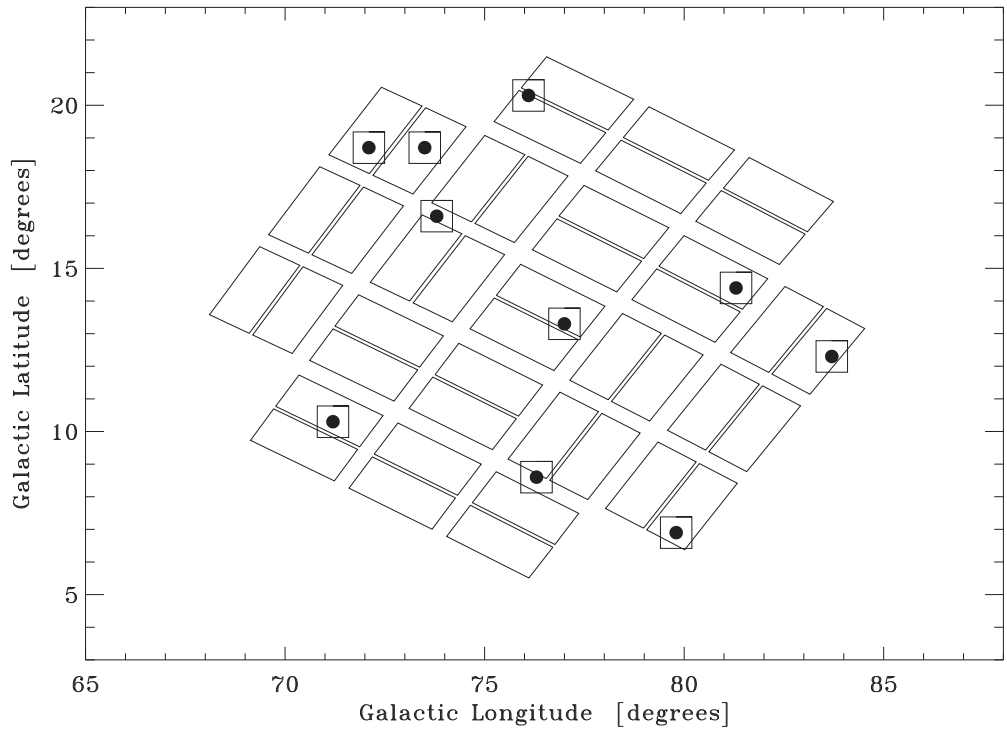

Figure 4. Ten pointings used for the TRILEGAL galaxy model in order to construct the simulated samples discussed in the text. Each run of the TRILEGAL program was a 1.0 deg^2 simulation, as indicated by the size of the box around each point. The outline of the *Kepler* CCDs is shown by rectangular shapes drawn with solid lines.

about 3000–10,000 K, it is dominated by dwarfs that have near-solar values in both quantities.

3. METHOD

We wish to study the number of bound versus the line-of-sight companions that will be detected by the DSSI instrument when looking at stars randomly selected in the *Kepler* field. The vast majority of *Kepler* stars are in a distance range of roughly 200–1000 pc relative to the solar system (corresponding to a diffraction-limited separation of 10–50 AU at WIYN, and 4–20 AU at Gemini North). The range of Galactic latitude and longitude appropriate for the *Kepler* field is $5\overset{\circ}{.}5 \leqslant b \leqslant 21\overset{\circ}{.}48$ and $68\overset{\circ}{.}1 \leqslant l \leqslant 84\overset{\circ}{.}5$, respectively.

We have used the TRILEGAL galaxy model (Girardi et al. 2005) to construct simulations of star counts in the *Kepler* field of view. Ten randomly selected pointings within the *Kepler* field were used; these are shown in Figure 4. This produced 10 lists of stars, which were then combined to give better statistical results of the properties of the stars in the entire field. Each of the 10 simulations had a field of view of one square degree, but the simulations were run with the binary parameters turned off. Since for this study we required detailed information regarding the companion stars and their orbital properties, these were added after the fact as follows. From the TRILEGAL output, we constructed a distance-limited sample with maximum distance from the solar system of 1300 pc. In order to study only stars like those observed, we excluded stars with effective temperatures less than 3000 K and greater than 10,000 K, and also required that $\log(g)$ was between 3.3 and 4.7, although, since the observed sample had only a small percentage of higher-temperature stars (as can be seen from Figure 3), we removed, at random, 50% of those stars with effective temperature greater than 7000 K.

As this was a distance-limited sample overwhelmingly dominated by solar-type stars, it is reasonable to add companions according to the known statistics of the field population of binaries (Duquennoy & Mayor 1991; Raghavan et al 2010). Specifically, we populate the stars in the sample with companions at the rate of 46%. We find a mass ratio for each system by utilizing the mass-ratio distribution found in Raghavan et al. 2010 (specifically, Figure 16 in that work). The mass of the primary is known from the TRILEGAL output, so the secondary mass is then calculated. From the mass–luminosity relation of Henry & McCarthy (1993), these masses can be converted into absolute V magnitudes. Using the distance, an apparent magnitude can be calculated as well as a magnitude difference for the binary components. Finally, we convert this magnitude difference at V to the speckle 692 nm filter by estimating the spectral type of the primary and secondary from the mass values and using the known filter transmission curves.

In the case of binary stars, we select a period according to the Duquennoy & Mayor (1991) log-normal period distribution, and an eccentricity for the orbit using the information in the same paper. We select random values for the cosine of the inclination ($\cos i$), ascending node (Ω), and the angle in the true orbit between the line of nodes and the semi-major axis (ω), and time of periastron passage (T). Finally, we determine the semi-major axis in AU from the masses and the period and convert this to arcseconds using the distance. With the seven orbital parameters in hand, we can then compute the ephemeris position angle and separation for a randomly chosen epoch of observation.

We then test whether a companion would be detected for each star in the sample using the camera and telescope combinations from our work (whether single or double). In order to make this determination, we first select stars that have an apparent magnitude brighter than the detection limit for the telescope in question (14.5 at WIYN, 16.5 at Gemini North). We assume that single stars would be seen as single by DSSI, but for binaries, we next apply an average contrast limit curve for WIYN and

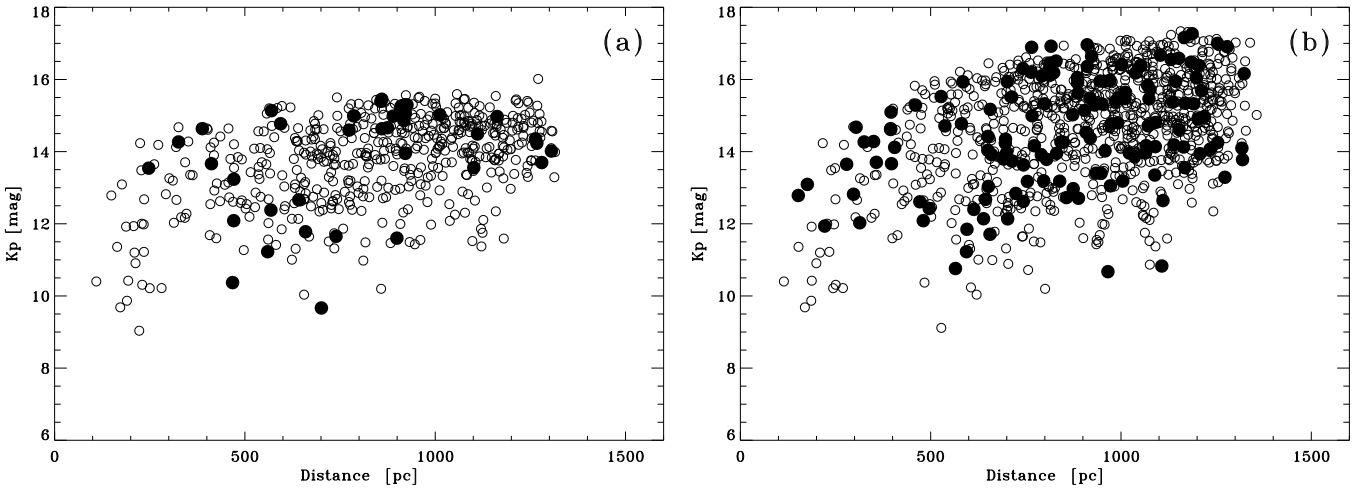

Figure 5. *Kepler* magnitude as a function of estimated distance for the simulation results for (a) WIYN and (b) Gemini. Open circles represent stars with no detection of a companion, and filled circles represent stars with detected companions.

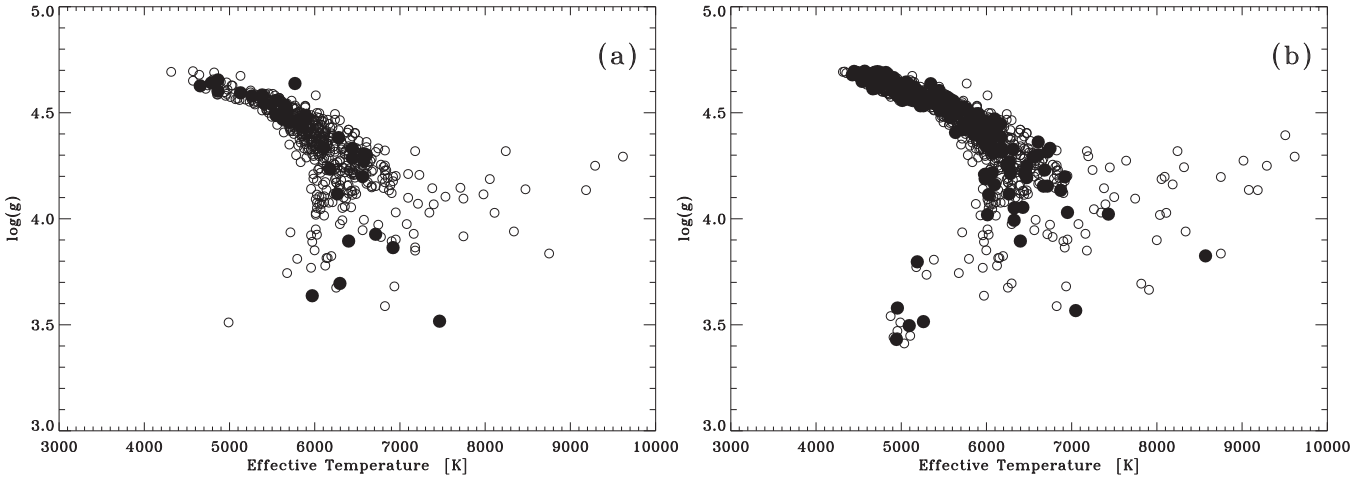

Figure 6. Surface gravity [log(g)] as a function of effective temperature for the simulation results for (a) WIYN and (b) Gemini. Open circles represent stars with no detection of a companion, and filled circles represent stars with detected companions.

Gemini, that is, a curve of the maximum observable magnitude difference as a function of separation from the central star. The process for making detection limit curves for *Kepler* has been described in, e.g., Howell et al. (2011) and Horch et al. (2011), but briefly, we use the reconstructed (i.e., diffraction-limited) images from the speckle data in order to estimate such curves for all stars observed. We determine the values of all the local maximum "sky" pixels within a set of concentric annuli centered on the target star. Detection limits for a point source at a given radius are calculated using the appropriate annulus and are set to the mean of the maxima plus five times the standard deviation of the maxima. If its magnitude difference is less than the value of this curve for the separation of the system, then a companion is considered to be detectable.

DSSI is essentially a magnitude-limited instrument at each telescope, sensitive to targets brighter than $V \sim 14.5$ at WIYN and 16.5 at Gemini, although these boundaries are influenced somewhat by observing conditions. Because of this fact, we anticipate that some binaries where both stars' magnitudes lie below the detection threshold will be nonetheless detectable due to the combined light, thereby creating a potential bias due to faint, primarily small-magnitude-difference pairs. However, because the simulations are first distance-limited, and then binaries are added to this entire sample before imposing the detection limit of the camera, the simulation results also reflect this bias. For example, in the WIYN simulations, about 15% of binaries detected had both primary and secondary magnitudes below the detection threshold, and for Gemini, the result was about 6%. (It is lower in this case due to the fact that the sample is dominated by G dwarfs within ∼1000 pc, and generally have apparent magnitudes well above the Gemini detection limit for the relevant range of distances.) Therefore, we have accounted for the observational bias by in effect building the same bias into the simulations.

The result of this simulation scheme is shown in Figures 5 and 6 for both WIYN and Gemini North. Figure 5 shows the *Kepler* magnitude of the sample as a function of distance and may be directly compared with Figure 2, while Figure 6 shows a plot of log(g) versus effective temperature, and may be compared with Figure 3. Only 1 of the 10 pointings in the *Kepler* field was used to make Figures 5 and 6 in order to keep the figures clear; In Figure 7, we show histograms of effective temperature and log(g) for the observed sample of stars at WIYN along with histograms of the complete "observable" sample from the WIYN simulation, including all 10 pointings. (Plots for Gemini appear very similar, but with many fewer observations and much lower statistical significance.) On this basis, we judge these simulated samples to be sufficiently close to the actual

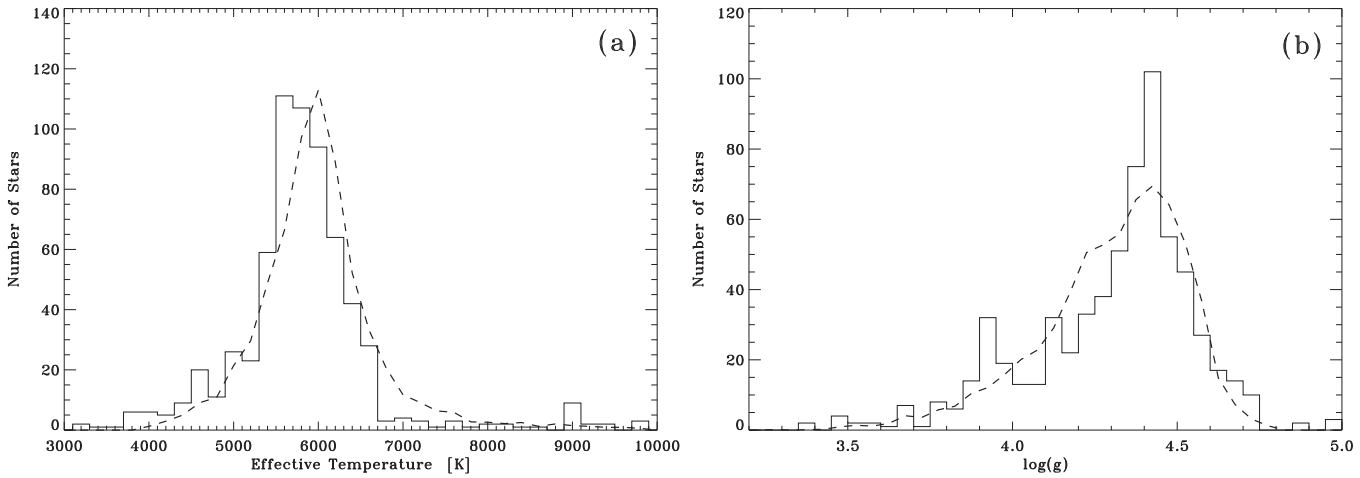

Figure 7. Histograms of (a) effective temperature and (b) surface gravity [log(g)] for the observed WIYN sample of *Kepler* stars (solid line) vs. the entire observable sample of simulated stars (dashed line). The simulated results have been normalized to the total number of stars in the observed sample.

observed samples in magnitude, distance, and stellar make-up to be useful in predicting the percentage of detected companions at each telescope with the speckle instrument. Given this approach, the periods for the detected binaries in the Gemini simulation ranged from 17 to 376,000 yr, with a median value of 970 yr. For the WIYN simulation, the minimum period was 29 yr, the maximum was 49,400 yr, and the median value was 1600 yr.

To determine the frequency of optical doubles (i.e., line-of-sight components), we assigned random positions within the field to the stars in the output file of each TRILEGAL simulation, and then computed the distance on the sky between these stars and each of the previously identified observable stars. For stars that had a separation of less than 1.2 arcsec, we computed a magnitude difference, and use the contrast limit curves to determine if the object would be seen as double when observed with the speckle camera.

4. RESULTS

Using the simulations described above, we can now compare to the observed data in terms of the properties of detected components. In Figures 8 and 9, we show the magnitude difference of all detected and simulated binaries as a function of separation. We also plot the average detection limits at 692 nm as a function of separation used for this study for WIYN and Gemini North, respectively. For the observed data, the percentage of KOIs where companions were discovered at WIYN is 7.0% ± 1.1% (41 of 588 targets observed), whereas for Gemini it is 22.8% ± 8.1% (8 of 35 targets observed).

Note that in Figure 8 there are seven systems that are above the contrast limit curve. The curve we have selected for the analysis here is an average of several obtained from unresolved objects that have apparent magnitudes comparable to the normal range of *Kepler* objects observed at WIYN, between 11th and 14th magnitude. However, some *Kepler* stars are significantly brighter than this, and so would have much higher signal-to-noise than the typical *Kepler* observation. In addition, the contrast limit curve will be higher for objects taken in better seeing conditions. It is not uncommon to detect companions at magnitude differences of 5 at WIYN for brighter targets observed in good seeing (see, e.g., Horch et al. 2011). So, while there is some variation in the detection limit curves for individual observations, the curve shown is a reasonable average for *Kepler* observations. Without the seven detections shown above the detection limit curve that is drawn (and all seven represent sources brighter than magnitude 12.2), then the observed rate of companion detection at WIYN would be 5.8% ± 1.0%. However, this number is likely to be an underestimate of the true WIYN detection rate for the detection limit curve shown, as some stars would have been observed in poor conditions where fainter companions below the detection limit curve would still be missed. In contrast, the same situation does not exist at Gemini, since the larger telescope aperture puts nearly all *Kepler* stars observed to date into the high signal-to-noise regime.

Also in Figures 8 and 9, we show the simulation results obtained as described in Section 2, where the detection limit curves shown in Figures 8 and 9 are assumed. We find that, in the case of WIYN simulations, the percentage of detected companions predicted is 7.8% ± 0.4% (451 of 5745 trials). Of these companions, 96% are predicted to be bound companions (with the remaining 4% being optical doubles). In the case of Gemini data, the rate of companion detection is predicted to be 19.7% ± 0.4% (2148 of 10,879 trials), 84% of which are predicted to be gravitationally bound systems, 94% of systems with $\Delta m < 5$ are gravitationally bound.

In both cases, we find reasonably good agreement with the observed rate of detections when assuming the 46% number for stars with companions from Raghavan et al. 2010. (That is, we are using 7.1% ± 1.1% observed for WIYN versus 7.8% ± 0.4% predicted and 22.8% ± 8.1% observed for Gemini versus 19.7% ± 0.4% predicted.) These numbers give confidence that our detection limits are well-understood. In Figures 8 and 9, it is interesting to note the segregation of the two types of companions particularly in the Gemini simulation, with most line-of-sight companions being at larger separations and higher magnitude differences. In contrast, the bound stellar companions cluster toward smaller separations, with typical semi-major axes of $\lesssim$90 AU (periods less than ~700 yr).

To make a preliminary statement regarding the binarity of exoplanet host stars, we first remove from the above statistics those objects judged to be false positives as of the present. This gives us the cleanest possible sample of exoplanet candidate host stars with which to work. In this case, the WIYN detection rate is reduced to 6.2% ± 1.1% (32 of 518 stars), slightly below that of the simulations, while the Gemini detection rate remains fairly constant and consistent with the simulations, at 20.0 % ± 8.2% (6 of 30 stars). We have redone the simulations, changing the input rate of companions to see what effect that would have

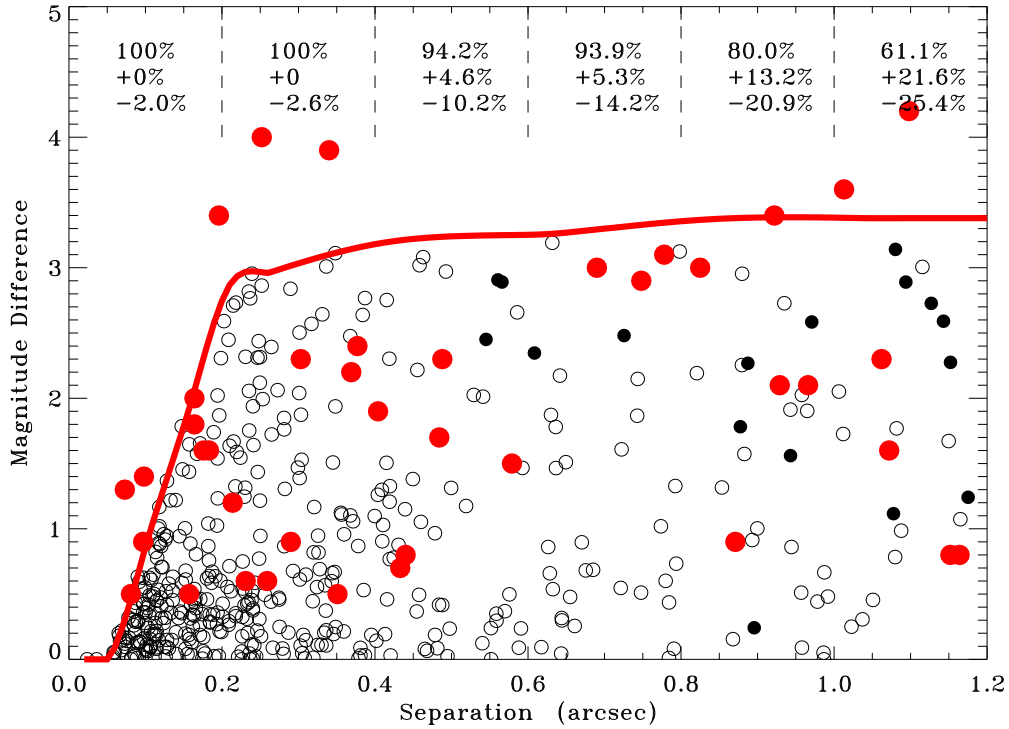

Figure 8. Simulation results for predicted stellar detections and observational results for WIYN at 692 nm. The open circles represent detected bound components and the filled black circles represent detected line-of-sight components from the simulation. The filled red circles are the locations on the diagram of components discovered at WIYN and the red curve is the average-quality detection curve appropriate for *Kepler* stars. The numbers shown along the top of the diagram are the percentage of bound companions for each 0.2 arcsec wide bin in separation. The uncertainties represent a 95% confidence interval.

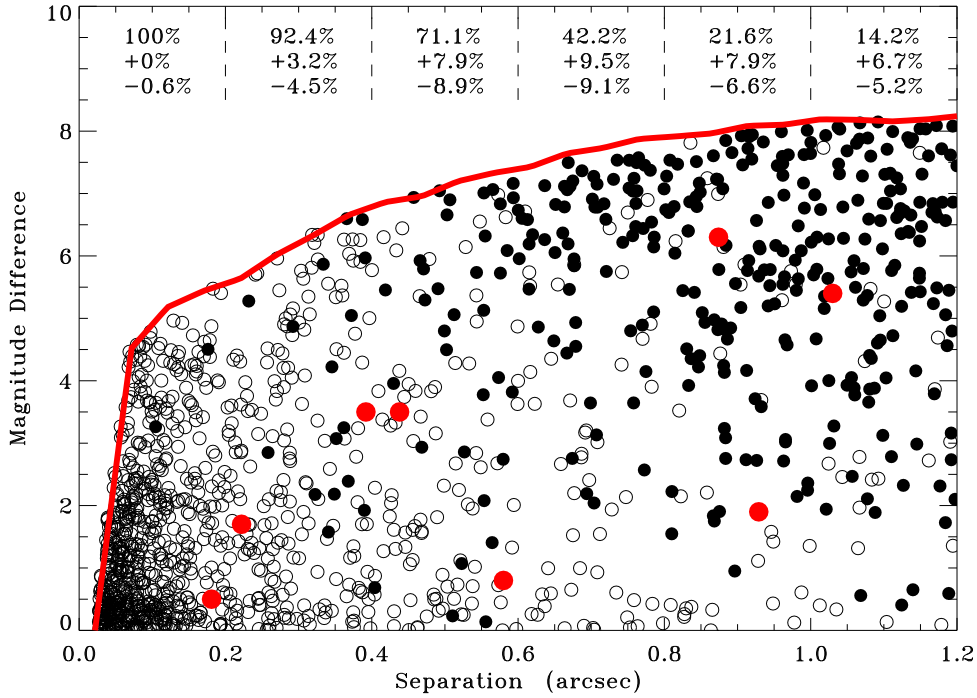

Figure 9. Simulation for predicted stellar detections and observational results for Gemini at 692 nm. The open circles represent detected bound components and the filled black circles represent detected line-of-sight components from the simulation. The filled red circles are the locations on the diagram of components discovered at Gemini and the red curve is the average-quality detection curve appropriate for *Kepler* stars. The numbers shown along the top of the diagram are the percentage of bound companions for each 0.2 arcsec wide bin in separation. The uncertainties represent a 95% confidence interval.

on the final prediction for companion detection. From this, we can estimate that the companion star fraction of this "clean" sample at WIYN is 37% ± 7% at present. A similar study of Gemini data resulted in an estimate of the companion star fraction of 47% ± 19%. These numbers bracket the 40%–50% range believed to be the case for field stars.

5. DISCUSSION

5.1. General Comments

The Duquennoy & Mayor log-normal period distribution for binary stars has its peak at a period of 180 yr for G type stars; there is less information in the literature about other

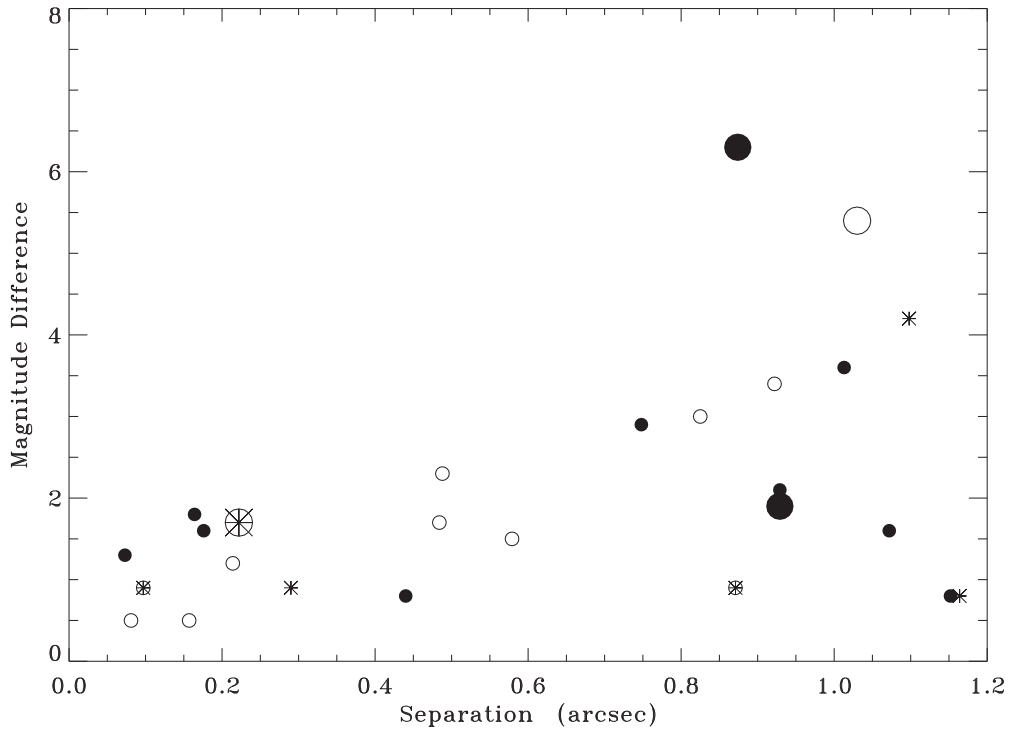

Figure 10. Magnitude difference vs. separation for KOI speckle double stars that have been subsequently identified as false positives (filled circles) and multi-planet candidate systems (open circles). Validated systems are shown with an asterisk symbol. Objects observed at Gemini North are shown with plot symbols that are twice as large as for WIYN data points.

spectral types. Nonetheless, if the distribution is similar for main sequence spectral types A–M, the data indicate that, even at Gemini with its much more sensitive detection limits, most observed close companions will be gravitationally bound.

It is estimated that, in general, over 90% of KOI stars do indeed harbor transiting exoplanets, i.e., the false positive rate is thought to be under 10% (Morton & Johnson 2011; Fressin et al. 2013; Santerne et al. 2013), though it is generally believed that the presence of a companion increases the false positive probability due to the possibility of the companion being a background eclipsing binary star. Likewise, the identification of multiple planet candidates and/or the orbital period of a planet candidate also can decrease the false positive rate (Lissauer et al. 2014). For truly bound companions detected here it is not clear that the false positive rate should increase, since an eclipsing binary bound to the KOI star would contribute more light in general than a background system and would therefore be more likely to have deeper transit-like events in the *Kepler* data stream. It would be more easily recognized as a false positive. Combining this line of thinking with the results obtained here, it implies that the sample of detections shown in Figures 8 and 9 is mainly comprised of binary systems where one of the stars harbors an exoplanet. Since the binary statistics derived here come from those of the known field population, it would appear that, for the full range of separations and periods to which we are sensitive, the binary fraction of stars that have exoplanets is overall roughly consistent with that of the field population. Otherwise our observed detection rates would not match those of the simulations.

5.2. Further Vetting

Since their identification as KOIs, 11 of our 49 discoveries have been judged to be false positives (see Batalha et al. 2013; Burke et al. 2014), while 12 other targets have been identified as multi-planet candidate systems (see, e.g., Lissauer et al. 2014), and 6 have been validated as exoplanet hosts, 2 with multi-planet systems (see, e.g., Marcy et al. 2014; Rowe et al. 2014). While we do not yet have sufficient speckle data in hand to study the placement of the components of these systems farther on the H-R diagram, we can at least note the positions of these objects in a plot like Figures 8 or 9 and investigate the implications of this considering where line-of-sight and bound companions are expected to dominate the sample. This is shown in Figure 10. We see that the two false positives from the Gemini list and five from the WIYN list do have positions that put them in the region populated by light-of-sight companions, whereas zero Gemini and four WIYN false positives are in a region dominated by bound companions. In contrast, 8 out of 12 of the multi-planet candidate systems occur in the region of separation less than 0.6 arcsec and magnitude differences less than 2.5. Only one of the validated systems lies in a region where more line-of-sight companions are expected. The sample size is still very low, so firm conclusions cannot be made; however, at this stage there is no obvious inconsistency, as, e.g., one would expect false positives to be generated by background stars in many cases.

If the known false positives are discounted, then we are left with a sample of 38 KOIs with companions detected with speckle imaging, 6 of which have already been validated as hosting exoplanets. While it is true that it is still possible for some of these systems to be judged to be false positives in the future, the false positive rate is not likely to be worse than the standard 10% number discussed above, which would imply that roughly 35 or more of the sample are gravitationally bound binaries that host exoplanets.

5.3. Planet Radius

The speckle observations and companion modeling indicate that any star detected within ∼1 arcsec is almost certainly a

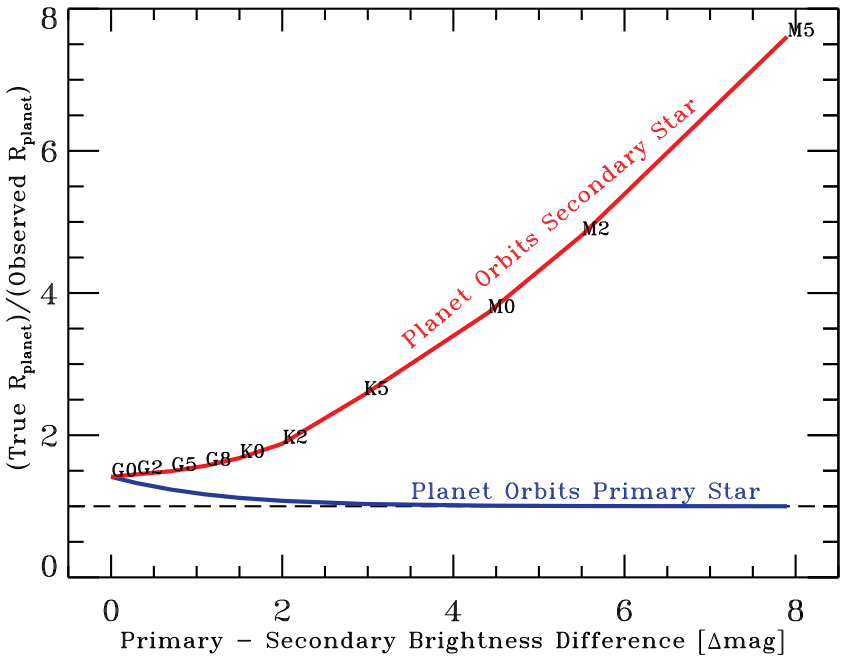

Figure 11. Ratio of the true planet radius to the observed planet radius for a blended binary as a function of *Kepler* magnitude difference between the companions. The blue line represents the ratio if the planet orbits the primary star; this line is the same for all stars regardless of spectral type because the derived radius is only affected by the transit dilution of the secondary star (i.e., the presumed stellar radius does not change significantly). The red line represents the ratio if the planet orbits the secondary star and takes into account the brightness deblending and the difference in the stellar radii between the primary and secondary stars. The positions of the possible secondary stars are marked in black. The exact shape of this line is dependent upon the primary stellar type as the secondary star, by definition, will be fainter and smaller than the primary. In this example, the primary star is a G0V.

bound companion star. If a target star is blended with another star (bound or line-of-sight), the true planet radius is larger than the derived planet radius because the observed transit depth is diluted by the companion star. In general, we do not know around which star the planet is orbiting. If the primary star hosts the planet, then for an equal brightness binary (assuming no color difference), the planet size is underestimated by no more than a factor of $\sqrt{2}$ and as the binary ratio (and hence, relative brightness) increases, the observed planet radius asymptotically approaches the true planet radius. This is shown in the blue line of Figure 11.

If we assume that the companion star is indeed bound as indicated by the simulations above, then the secondary star must be smaller than the primary star (i.e., a lower luminosity indicates a smaller star). If the planet orbits the secondary star, the planet can be significantly larger than anticipated because the secondary star is heavily diluted by the primary star *and* the secondary star is smaller than the primary star (i.e., the stellar radius assumed if the planet orbited the primary star). As an example, in the red line in Figure 11, we have calculated the change in the derived planet radius for a G0V primary star with a bound companion of some stellar type, but it is the companion that hosts the planet. Correcting for the transit dilution and the smaller stellar radius of the secondary star, the true planet radius can be 1.4–8.0 times larger than the planet radius derived from the blended photometry and assuming the planet orbits the primary star: the fainter the companion, the larger the planet actually is. There is, of course, a limit such that an observed transit depth cannot be mimicked by a star if the star is too faint and/or the transit depth is too deep.

We have taken the known effective temperatures, magnitude differences, and planet radii (as appearing on the CFOP Web site) of the 49 double stars in our sample and estimated spectral types for the secondary star using information in Schmidt-Kaler (1982). Then, using curves like Figure 11, we have estimated the factor by which the true planet radius is larger than that derived from the transit data if the planet were to orbit the secondary star. The result is that 28 of 41 WIYN discoveries (68%) have planet radii that remain well below the threshold of a late M-dwarf even if orbiting the secondary, and all 8 Gemini discoveries (100%) remain below the stellar threshold in radius. In the WIYN sample, 9 of the 41 stars are now judged to be false positives; five of these are in the group of 13 stars that do not remain below the stellar radius threshold in this exercise, a significant overlap. We conclude that it is not possible to explain the majority of transits by suggesting that the secondary is an eclipsing binary star.

5.4. Possible Suppression of Small-separation Stellar Components

The study of Wang et al. (2014b) concluded that there is a suppression of stellar companions inside 20 AU for exoplanet host stars. In the range from 20 to 85 AU, the data were less clear-cut, and above 85 AU, the binary fraction appeared to be consistent with that of the field population. The work here is mainly sensitive to separations above 20 AU since the vast majority of objects detected in the simulations have semi-major axes greater than this value (only 32 stars of 1796 detections in the Gemini simulation and 4 of 538 in the WIYN simulation have a semi-major axis less than 20 AU.) However, 35.2% of detected binaries in the Gemini simulation and 16.4% of those detected in the WIYN simulation have semi-major axes in the range of 20–85 AU. If there were a reduction of, e.g., 50% in stellar companions in this range, then the overall predicted Gemini detection rate would be reduced only to 16.8% while the overall WIYN rate would drop to 7.6%.

Both of these values are still consistent with the observed values at present, but we note that objects with semi-major axes

less than 85 AU predominantly occur at observed separations less than 0.2 arcsec(74 of 184 objects for the WIYN simulation and 657 of 1139 objects in the Gemini simulation have both observed separation less than 0.2 and semi-major axis less than 85 AU). Thus, if there were a suppression of binaries with $a < 85$ AU, this could be seen in a relative lack of detected components at separations less than 0.2 arcsec. For WIYN, the simulation results predict that if no such suppression exists, then 41% of detections should be made at separations less than 0.2 arcsec. Using our "clean" sample from the Section 5.3, out of 32 binaries at WIYN, we would therefore expect 13 ± 4 detected below 0.2 arcsec, whereas for our sample 7 have been detected. For Gemini, the simulation indicates that 53% of companions detected should have separations below 0.2 arcsec, or in a sample of 6, about 3 ± 2, whereas only one object so far as been detected in this category. The sample sizes preclude definitive statements at this point, but clearly with continued observations of the KOI targets, there is an opportunity to investigate this important range of semi-major axes.

A second paper by Wang et al. (2014a) indicates a potentially much broader but weaker suppression of stellar companions for exoplanet host stars, out to separations as large as 1500 AU. These results are based on a combination of adaptive optics and radial velocity observations. Our results include this larger range of distances, but neither the Wang et al. result nor our work have small enough uncertainties at this stage to be definitive. While Wang et al. break their results down by physical separation and we do not, our results for the value of the companion star fraction quoted in Section 4 for the "clean" exoplanet host star sample are easily less than 2σ from their number at 100 AU, and our number is consistent with the Wang et al. result at 1000 AU. In addition, the possible lack of small separation components in our case is broadly in line with their findings, though it is difficult to quantify at this stage. We conclude that high-resolution imaging techniques (speckle imaging, lucky imaging, and adaptive optics) represent an extremely important way to detect small separation companions and assess the true binary fraction of exoplanet host stars. Of these techniques, speckle imaging at Gemini offers the highest spatial resolution (20 mas), and will overlap to the greatest extent with radial velocity studies. Finding a companion to a KOI star typically corresponds to the identification of a binary host star with one or more exoplanets. Our continued observations of *Kepler* and other exoplanet host stars will provide high-precision magnitudes and colors of stellar components, eventually allowing us to use isochrone fitting to place the stars on the H-R diagram, as discussed in Davidson et al. (2009). Such analyses can yield mass information of the components, and if one component is evolved, to estimate the age of such systems.

6. CONCLUSIONS

We have simulated the detection process for speckle imaging of *Kepler* Objects of Interest and compared the rate of companions predicted with that found so far in real observations. We find that the real rates of companion detection are, within uncertainties, the same as the simulations for two different speckle observing situations, the WIYN telescope and Gemini North. The simulations incorporate the TRILEGAL galaxy model to generate lists of stars and their properties in the *Kepler* field. After a distance-limited subsample of these objects is constructed, the known statistics concerning binarity among stars near the Sun is added. The simulations predict that the very large majority of sub-arcsecond companions will be physically bound to the *Kepler* star. This result suggests that, over the separation range to which we are sensitive, exoplanet host stars have a binary fraction consistent with that of field stars. Our speckle imaging program has identified a sample of candidate binary-star exoplanet systems in which only a modest number of false positives are likely to exist.

We thank the *Kepler* Project Office located at the NASA Ames Research Center for providing partial financial support for the upgraded DSSI instrument. It is also a pleasure to thank Steve Hardash, Andy Adamson, Inger Jorgensen, and the entire summit crew for their assistance at Gemini, as well as Charles Corson and the team of observing assistants at WIYN for all of their help during our runs over the last few years. We also thank the anonymous referee for her/his comments that have helped to significantly improve the paper. This work was funded by the *Kepler* Project Office.

REFERENCES

Adams, E. R., Ciardi, D. R., Dupree, A. K., et al. 2012, AJ, 144, 42
Batalha, N. M., Rowe, J. F., Bryson, S. T., et al. 2013, ApJS, 204, 24
Borucki, W. J., Koch, D. G., Basri, G., et al. 2011, ApJ, 728, 117
Burke, C. J., Bryson, S. T., Mullally, F., et al. 2014, ApJS, 210, 19
Davidson, J., Baptista, B. J., Horch, E. P., Franz, O., & van Altena, W. F. 2009, AJ, 138, 1354
Duquennoy, A., & Mayor, M. 1991, A&A, 248, 485
Everett, M. E., Howell, S. B., Silva, D. R., & Szkody, P. 2013, ApJ, 771, 107
Fressin, F., Torres, G., Charbonneau, D., et al. 2013, ApJ, 766, 81
Girardi, L., Groenewegen, M. A. T., Hatziminaoglou, E., & da Costa, L. 2005, A&A, 436, 895
Henry, T. J., & McCarthy, D. W. 1993, AJ, 106, 773
Horch, E., Falta, D., Anderson, L. M., et al. 2010, AJ, 139, 205
Horch, E., Gomez, S. C., Sherry, W. H., et al. 2011, AJ, 141, 45
Horch, E., Howell, S. B., Everett, M. E., & Ciardi, D. R. 2012, AJ, 144, 165
Horch, E., Veillette, D. R., Baena Gallé, R., et al. 2009, AJ, 137, 5057
Howard, A. W., Marcy, G. W., Bryson, S. T., et al. 2012, ApJS, 201, 15
Howell, S. B., Everett, M. E., Sherry, W., Horch, E., & Ciardi, D. R. 2011, AJ, 142, 19
Huber, D., Silva Aguirre, V., Matthews, J. M., et al. 2014, ApJS, 211, 2
Kraus, A. L., Ireland, M. J., Hillenbrand, L. A., & Martinache, F. 2012, ApJ, 745, 19
Lissauer, J. J., Marcy, G. W., Bryson, S. T., et al. 2014, ApJ, 784, 44
Marcy, G. W., Isaacson, H., Howard, A. W., et al. 2014, ApJS, 210, 20
Morton, T., & Johnson, J. 2011, ApJ, 738, 170
Parker, R. J., & Quanz, S. P. 2013, MNRAS, 436, 650
Raghavan, D., McAlister, H. A., Henry, T. J., et al. 2010, ApJS, 190, 1
Rowe, J. F., Bryson, S. T., Marcy, G. W., et al. 2014, ApJ, 784, 45
Santerne, A., Fressin, F., Días, R. F., et al. 2013, A&A, 557, 139
Schmidt-Kaler, T. 1982, in Landolt-Börnstein New Series, Group 6, Vol. 2b, Stars and Star Clusters, ed. K. Schaifers & H.-H. Voigt (Berlin: Springer), 1
Wang, J., Fischer, D. A., Xie, J.-W., & Ciardi, D. R. 2014a, ApJ, 791, 111
Wang, J., Xie, J.-W., Barclay, T., & Fischer, D. A. 2014b, ApJ, 783, 4
Xie, J.-W., Zhou, J.-L., & Ge, J. 2010, ApJ, 708, 1566